Coverage Probability Density: A Spatially-Resolved Performance Analysis for Non-Homogeneous Maritime Networks

Wen-Yu Dong, Shaoshi Yang, *Senior Member, IEEE*, Jinyang Yu, Song Zhao, Weiliang Xie, Rui-Si Han, Qi Bi, *Fellow, IEEE*, and Sheng Chen, *Life Fellow, IEEE*

***Abstract*—The performance analysis of maritime communication networks is frequently constrained by the widespread yet unrealistic assumption of a uniform spatial distribution of vessels. This paper presents a unified stochastic geometry framework that integrates high-fidelity physical channel models with non-homogeneous vessel topologies to provide a more accurate analytical foundation. We first systematically demonstrate that the macroscopic geographical distribution of vessels is a dominant factor governing overall network performance, with significant performance variations observed across different deployment scenarios. Subsequently, to analyze the spatial origins of this performance, we introduce the coverage probability density function (Cpdf) as a novel metric. The Cpdf enables a fine-grained spatial decomposition of the total coverage probability, thereby identifying key geographical areas that contribute most to network performance and quantifying the precise spatial impact of physical phenomena, such as multipath fading nulls. Our results affirm the primacy of realistic spatial modeling and provide a new analytical tool for the design and optimization of next-generation maritime networks.**

***Index Terms*—Stochastic geometry, maritime communication, non-homogeneous Poisson point process, coverage probability density.**

I. Introduction

The ongoing digitalization of the maritime industry has elevated the importance of reliable near-shore wireless communication, which now constitutes critical infrastructure for ensuring navigational safety and enabling intelligent shipping applications [1, 2]. A rigorous performance evaluation of such networks, however, faces a significant analytical challenge: the development of a tractable model that jointly captures the complex maritime channel physics and the realistic geographical distribution of users.

The maritime propagation environment is characterized by unique physical phenomena, including sea-surface reflection and evaporation ducting, which are not adequately described by simplistic path loss models [3]. Concurrently, the spatial distribution of vessels is inherently non-homogeneous, exhibiting clustering near ports and along major shipping lanes. Consequently, the common analytical assumption of a uniform spatial distribution, while mathematically convenient, leads to considerable inaccuracies in network performance evaluation [4].

A review of the existing literature reveals a persistent gap between two areas of research. While stochastic geometry is a powerful tool for wireless network analysis, a significant gap exists in its application to maritime communications. Current shore-to-vessel analyses often employ overly simplistic spatial models, such as assuming a uniform vessel distribution or analyzing a single representative link [5, 6]. Although more complex non-homogeneous Poisson point processes (NHPPPs) exist, they typically rely on structured models like Poisson cluster processes [7–9], which are ill-suited for the arbitrary patterns of maritime traffic. This issue is compounded by the prevalent use of simplified large-scale path loss models. For example, some analyses use empirical International Telecommunication Union (ITU) models [5], while others adopt a standard power-law [6]. These models lack physical fidelity and fail to capture the unique propagation characteristics of the near-shore environment. In contrast, physics-based piecewise models [10] offer greater accuracy and analytical tractability, enabling the precise analysis of phenomena like deep fading nulls. The widespread use of these simplified spatial and path loss models underscores the absence of a comprehensive framework that integrates a general, arbitrarily shaped NHPPP with a high-fidelity, physics-based channel model for the accurate analysis of large-scale maritime networks.

This paper addresses this analytical gap by advancing a central thesis with two key components. We first establish that the macroscopic geographical topology is the dominant factor governing network performance. Subsequently, we address the insufficiency of conventional single-value metrics by introducing the coverage probability density function (Cpdf), a spatially-resolved metric designed to characterize the underlying geographical dynamics of network performance. Our work includes the following contributions.

This work is supported by National Science and Technology Major Project–Mobile Information Networks under Grant 2024ZD1300200. *(Corresponding author: Shaoshi Yang)*

W.-Y. Dong, J. Yu, S. Zhao and Q. Bi are with the Future Technology Research Center, China Telecom Research Institute, Beijing 102209, China (Email: dongwy@chinatelecom.cn; yujy10@chinatelecom.cn; zhaosong1@chinatelecom.cn; qibi@chinatelecom.cn)

S. Yang is with the School of Information and Communication Engineering, Beijing University of Posts and Telecommunications, and also with the Key Laboratory of Mathematics and Information Networks, Ministry of Education, Beijing 100876, China (E-mail: shaoshi.yang@bupt.edu.cn).

W. Xie is with the Mobile and Terminal Technology Research Department, China Telecom Research Institute, Beijing 102209, China (Email: xiewl@chinatelecom.cn)

R.-S. Han is with the Cloud Network Operating System R&D Center, China Telecom, Beijing 102209, China (Email: hanruisi@chinatelecom.cn)

S. Chen is with the School of Electronics and Computer Science, University of Southampton, Southampton SO17 1BJ, U.K. (E-mail: sqc@ecs.soton.ac.uk).

- A Unified Framework for Physics-Based, Large-Scale Analysis: We propose an analytical framework that integrates a physically-grounded piecewise path loss model with a general NHPPP, thereby closing a critical gap between oversimplified theoretical models and the reality of maritime communications.
- Establishing the Primacy of Macro-Topology: Through a systematic investigation of four distinct, physically-motivated spatial models, we definitively show that macroscopic geography is the primary determinant of network coverage and rate, providing a more realistic foundation for system design.
- A Novel Spatially-Resolved Diagnostic Metric: We introduce and formulate the Cpdf, a metric that disaggregates average network performance into a function of distance. We demonstrate its utility in identifying key geographical regions of optimal performance and in quantifying the localized impact of physical phenomena, such as multipath fading nulls, which are otherwise obscured by conventional metrics.

II. System Model

We consider the downlink of a near-shore maritime network with a single onshore station (OS) at the origin serving vessels modeled by a spatial point process. The system operates in a noise-limited regime, which is a valid assumption for a single-transmitter scenario. For clarity, the key parameters and functions of the system model are summarized in Table I.

A. Topological Deployment: Modeling Vessel Locations

The spatial locations of all vessels are modeled by a NHPPP, Φ_{S}, on a 2D half-plane. A key assumption is that the distribution is radially symmetric, meaning the process intensity $\mu(d)$ depends only on the horizontal distance d from the OS. This intensity is modeled as:

$$\mu(d) = \mu_0 f(d), \tag{1}$$

where μ_0 is a baseline intensity constant, and $f(d)$ is a dimensionless spatial distribution function that captures how vessel density varies with distance. The choice of $f(d)$ allows us to model various realistic maritime traffic scenarios, which we explore in Section III.

TABLE I
Description of System Parameters and Functions

Parameter	Description
h_{t}	OS antenna height.
h_{r}	Vessel antenna height.
λ	Carrier wavelength.
d	Distance from the OS.
d_{break}	Path loss breakpoint.
d_{LOS}	Max LOS distance.
$\mu(d)$	Vessel intensity (density) at distance d.
$f(d)$	Vessel spatial density function.
$g(d)$	Vessel distance PDF.
$PL(D)$	Large-scale path loss.
$\lvert h\rvert^2$	Small-scale fading power gain.
P_{OS}	OS transmit power.
N_0	AWGN power.
T	SNR threshold.
P_{cov}	Average coverage probability.
$\mathcal{C}_{\text{pdf}}(d)$	Coverage PDF.

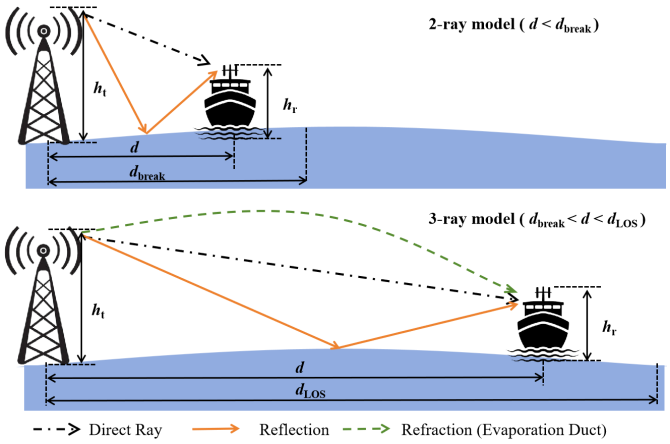

Fig. 1. Illustration of the near-shore maritime communication system.

B. Channel Fading and Path Loss Model

1) Small-Scale Fading: The near-sea-surface channel is characterized by a strong line-of-sight (LOS) path combined with scattering from the rough sea surface. We adopt the Nakagami-m fading model due to its flexibility and tractability. The channel power gain, $|h|^2$, follows a normalized Gamma distribution.

2) Large-Scale Path Loss Model: To accurately capture propagation physics, we employ a location-dependent, piecewise path loss model from [10], which transitions between two models at a breakpoint distance $d_{\text{break}} = 4h_{\text{t}}h_{\text{r}}/\lambda$, as illustrate in Fig. 1. Here, h_{t} and h_{r} are the antenna heights of the OS and the vessel, respectively, and λ is the wavelength.

- Two-Ray Model ($d < d_{\text{break}}$): At shorter ranges, the path loss is dominated by the coherent sum of the direct LOS path and a single sea-surface reflected path. This model accurately predicts interference nulls close to shore. The path loss is given by:

$$PL_{\text{2-ray}}(d) = \frac{(4\pi d)^2}{4\lambda^2 \sin^2\left(\frac{2\pi h_{\text{t}} h_{\text{r}}}{\lambda d}\right)}. \tag{2}$$

- Three-Ray Model ($d \geq d_{\text{break}}$): Beyond the breakpoint, a third path caused by reflection within the atmospheric evaporation duct becomes significant. This model provides superior accuracy at larger distances by capturing additional interference patterns. The path loss is:

$$PL_{\text{3-ray}}(d) = \frac{(4\pi d)^2}{4\lambda^2 \left(1 + \Delta(d)\right)^2}, \tag{3}$$

where $\Delta(d) = 2\sin\left(\frac{2\pi h_{\text{t}} h_{\text{r}}}{\lambda d}\right) \sin\left(\frac{2\pi (h_{\text{e}} - h_{\text{t}})(h_{\text{e}} - h_{\text{r}})}{\lambda d}\right)$ is the interference term, and h_{e} is the effective duct height.

C. SNR Model

In the downlink, the OS acts as the sole transmitter. Consequently, the link is interference-free, and its performance

is characterized by the signal-to-noise ratio (SNR) at the receiving vessel. The SNR is given by:

$$\text{SNR}_{\text{OS}} = \frac{P_{\text{OS}} \cdot |h|^2}{N_0 \cdot PL(D)}, \tag{4}$$

where P_{OS} is the transmit power of the OS, $|h|^2$ is the small-scale channel fading gain, $PL(D)$ is the large-scale path loss at distance D, and N_0 is the strength of additive white Gaussian noise (AWGN).

III. Spatial Distribution Models and Distance Analysis

The foundation of our analysis is the probability density function (PDF) of the distance d for a typical vessel, denoted as $g(d)$. Based on the assumption of radial symmetry, it is derived from the spatial distribution function $f(d)$ as follows:

$$g(d) = \frac{d \cdot f(d)}{\int_0^\infty \rho f(\rho) d\rho}. \tag{5}$$

The choice of $f(d)$ allows us to model diverse and realistic maritime traffic scenarios. We systematically investigate four distinct models.

A. Model 1: Piecewise Uniform Distribution (Harbors)

This model represents vessels constrained within a specific geographical area, such as a harbor or anchorage, between an inner radius D_{min} and an outer radius D_{max}. The function $f(d)$ is defined as:

$$f(d) = \begin{cases} 1, & D_{\text{min}} \le d \le D_{\text{max}}, \\ 0, & \text{otherwise.} \end{cases} \tag{6}$$

Substituting into (5), the distance PDF is:

$$g(d) = \begin{cases} \frac{2d}{D_{\text{max}}^2 - D_{\text{min}}^2}, & D_{\text{min}} \le d \le D_{\text{max}}, \\ 0, & \text{otherwise.} \end{cases} \tag{7}$$

B. Model 2: Exponential Decay Distribution (Coastal Traffic)

This model captures scenarios where vessel density is highest near the coast and decreases exponentially with distance, representing dense near-shore traffic. The function $f(d)$ is:

$$f(d) = e^{-kd}, \quad d \ge 0, \tag{8}$$

where $k > 0$ is the decay rate. The resulting distance PDF is a Gamma distribution with shape parameter 2 and decay rate k:

$$g(d) = k^2 d e^{-kd}, \quad d \ge 0. \tag{9}$$

C. Model 3: Power-Law Decay Distribution (Shipping Lanes)

To model major shipping lanes that extend far from shore, we use a heavy-tailed power-law decay distribution, which captures the slow decay of vessel density over vast distances. For normalizability, we require $\beta > 2$. The function $f(d)$ is:

$$f(d) = (d_0 + d)^{-\beta}, \quad d \ge 0, \tag{10}$$

where $d_0 > 0$ is an offset to prevent a singularity. The distance PDF is:

$$g(d) = \frac{d(d_0 + d)^{-\beta}(\beta - 1)(\beta - 2)}{d_0^{2-\beta}}, \quad d \ge 0. \tag{11}$$

D. Model 4: Annular/Gamma Distribution (Offshore Zones)

This flexible model represents scenarios where vessel density peaks at a certain distance offshore, such as in primary shipping lanes or designated operational zones. We use the functional form of a Gamma PDF for $f(d)$:

$$f(d) = d^{\alpha-1} e^{-\beta d}, \quad d \ge 0, \tag{12}$$

with shape $\alpha \ge 1$ and rate $\beta > 0$. The resulting distance PDF is also a Gamma distribution, but with a new shape parameter $\alpha + 1$:

$$g(d) = \frac{\beta^{\alpha+1}}{\Gamma(\alpha + 1)} d^\alpha e^{-\beta d}, \quad d \ge 0. \tag{13}$$

IV. Performance Analysis and Derivation

A. Average Coverage Probability

The coverage probability is the likelihood that the received SNR exceeds a threshold T. The *average* coverage probability, P_{cov}, is found by averaging the conditional coverage probability, $\mathbb{P}(\text{SNR}(d) > T)$, over the spatial distribution $g(d)$.

Theorem 1. *The average coverage probability for a typical vessel is given by:*

$$\begin{aligned} P_{\text{cov}}^{\text{DL}} = &\int_0^{d_{\text{break}}} \sum_{n=1}^{m} (-1)^{n+1} \binom{m}{n} \\ &\times \exp\left(\frac{-n\,\eta\,T\,N_0\,(4\pi d)^2}{4\,P_{\text{OS}}\,\lambda^2 \sin^2\left(\frac{2\pi h_{\text{t}} h_{\text{r}}}{\lambda d}\right)} \right) g(d)\,\mathrm{d}d \\ &+ \int_{d_{\text{break}}}^{d_{\text{LOS}}} \sum_{n=1}^{m} (-1)^{n+1} \binom{m}{n} \\ &\times \exp\left(\frac{-n\,\eta\,T\,N_0\,(4\pi d)^2}{4\,P_{\text{OS}}\,\lambda^2\,(1 + \Delta(d))^2} \right) g(d)\,\mathrm{d}d, \end{aligned} \tag{14}$$

where $d_{\text{break}} = \frac{4h_{\text{t}}h_{\text{r}}}{\lambda}$, $d_{\text{LOS}} = \sqrt{h_{\text{t}}^2 + 2h_{\text{t}}R} + \sqrt{h_{\text{r}}^2 + 2h_{\text{r}}R}$, $\Delta(d) = 2\sin\left(\frac{2\pi h_{\text{t}} h_{\text{r}}}{\lambda d}\right) \sin\left(\frac{2\pi(h_{\text{e}} - h_{\text{t}})(h_{\text{e}} - h_{\text{r}})}{\lambda d}\right)$, *and* $g(d)$ *is the PDF of the vessel distance, corresponding to one of the spatial distribution models defined in Section III*

Proof. The average coverage probability is the expectation of the conditional coverage probability over the user's spatial distribution, $g(d)$. Given the piecewise path loss model, this expectation is split at the breakpoint distance d_{break}:

$$\begin{aligned} P_{\text{cov}}^{\text{DL}} = &\int_0^{d_{\text{break}}} \mathbb{P}(\text{SNR}_{\text{2-ray}} \ge T | d) g(d)\,\mathrm{d}d \\ &+ \int_{d_{\text{break}}}^{d_{\text{LOS}}} \mathbb{P}(\text{SNR}_{\text{3-ray}} \ge T | d) g(d)\,\mathrm{d}d. \end{aligned} \tag{15}$$

The conditional probability $\mathbb{P}(\text{SNR} \ge T | d)$ is the probability that the channel power gain $|h|^2$ exceeds a threshold. Since $|h|^2$ is Gamma distributed, its CDF is $F_{|h|^2}(x) = 1 -$

$e^{-\eta x}\sum_{k=0}^{m-1}\frac{(\eta x)^k}{k!}$ for integer m. For tractability, we use a tight bound, yielding:

$$\mathbb{P}\left(|h|^2 > \frac{TN_0PL(d)}{P_{\text{OS}}}\right) \approx 1-\left(1-\exp\left(-\frac{\eta TN_0PL(d)}{P_{\text{OS}}}\right)\right)^m. \tag{16}$$

Using the binomial expansion $(1-x)^m = \sum_{n=0}^{m}\binom{m}{n}(-x)^n$, this is simplified to:

$$\mathbb{P}(\text{SNR} \geq T|d) = \sum_{n=1}^{m}(-1)^{n+1}\binom{m}{n} \times \exp\left(-\frac{n\eta TN_0PL(d)}{P_{\text{OS}}}\right). \tag{17}$$

Substituting the expressions for $PL_{\text{2-ray}}(d)$ and $PL_{\text{3-ray}}(d)$ from (2) and (3) into (17) and using the result in (15) completes the proof. □

B. Coverage Probability Density Analysis

While the average coverage probability P_{cov} provides a single, macroscopic measure of performance, its integrand, the Cpdf, reveals the underlying spatial dynamics. The Cpdf, $\mathcal{C}_{\text{pdf}}(d)$, is defined as:

$$\mathcal{C}_{\text{pdf}}(d) = \underbrace{\mathbb{P}(\text{SNR}(d) > T)}_{\text{Channel Quality Factor}} \times \underbrace{g(d)}_{\text{Geographic Factor}}. \tag{18}$$

This decomposition provides deep insights by showing that the performance contribution from any distance d is the product of two competing factors: the quality of the channel at that location (a microscopic, physical property) and the probability of finding a user there (a macroscopic, topological property). Analyzing the system through the lens of Cpdf offers several unique advantages over relying solely on an average value.

1) Deeper Insight and Identification of Sweet Spots: The Cpdf provides a spatially-resolved characterization of network performance by representing the contribution of each geographic distance to the overall average coverage probability. The peak of this density function identifies the critical distance where the combination of high user presence (a large value of $g(d)$) and reliable signal quality (high conditional coverage) is optimal. This analysis allows for a precise determination of which geographical regions contribute most to the overall performance and provides a basis for understanding why one spatial distribution may outperform another. For instance, a vessel distribution whose Cpdf peaks in a region of low path loss will yield a higher average performance.

2) Fading Nulls: A key strength of the Cpdf is its ability to resolve the spatial characteristics of physical layer phenomena. Unlike spatially averaged metrics that produce a smooth output, the Cpdf visualizes these geographic variations directly. For instance, the curve can exhibit sharp minima corresponding to locations that experience severe destructive multipath interference. These locations are commonly referred to as deep fading nulls.

In the considered near-shore VHF channel, these nulls are not numerical artifacts but rather inherent physical characteristics of the propagation environment. They arise from the destructive interference between the direct-path and sea-reflected-path signals. Within the framework of the two-ray model, this interference is maximized when the term $\sin^2\left(\frac{2\pi h_{\text{t}}h_{\text{r}}}{\lambda d}\right)$ in the path loss formulation approaches zero. Consequently, these nulls manifest at a discrete set of distances d_n from the transmitter, given by:

$$d_n = \frac{2h_{\text{t}}h_{\text{r}}}{n\lambda}, \quad \text{for } n = 1, 2, 3, \ldots. \tag{19}$$

Such deep fading nulls represent critical performance bottlenecks, creating localized zones of near-zero coverage. This granular, location-specific information is obscured by spatially averaged metrics like the overall coverage probability, P_{cov}. In contrast, the Cpdf explicitly reveals the precise locations and performance impact of these physical phenomena, thereby providing an invaluable diagnostic tool for network planning and optimization.

V. Simulation Results and In-depth Analysis

This section presents a detailed analysis of the simulation results, validating our theoretical framework and offering deeper insights into the performance of near-shore maritime communication networks. The results underscore the critical impact of spatial vessel distribution on network performance and demonstrate the diagnostic power of the Cpdf. Unless otherwise specifically stated, the default system parameters utilized in the simulations are listed in Table II.

A. Impact of Fading Severity on Coverage Probability

Fig. 2 illustrates the average downlink coverage probability as a function of the SNR threshold, T, for the four distinct spatial distribution models. Each subplot evaluates the performance across a range of Nakagami-m fading parameters, representing varying degrees of fading severity.

A consistent trend observed across all four spatial models is the inverse relationship between the coverage probability and the SNR threshold: as the required SNR threshold increases, the probability of achieving it naturally decreases. Furthermore, the results clearly validate the impact of the Nakagami-m parameter. Higher values of m, which signify less severe fading conditions, consistently yield a higher coverage probability for any given SNR threshold. Conversely, lower m values, corresponding to more severe fading, result in

TABLE II
Default Simulation System Parameters.

Notation	Parameters	Values
BS Transmit Power	P_{OS}	30 dBm
Noise Power	N_0	-100 dBm
Carrier Frequency	f	162 MHz
Nakagami-m Parameter	m	3
BS Antenna Height	h_{t}	50 m
Vessel Antenna Height	h_{r}	10 m
Evaporation Duct Height	h_{e}	30.5 m
Earth Radius	R_{earth}	6371 km
Piecewise Uniform Zone	$[D_{\min}, D_{\max}]$	[20, 30] km
Exponential Decay Rate	k	0.1
Power-Law Decay Exponent	β	2.5
Power-Law Offset Distance	d_0	8 km
Annular/Gamma Shape	α	1.5
Annular/Gamma Rate	β_γ	0.25

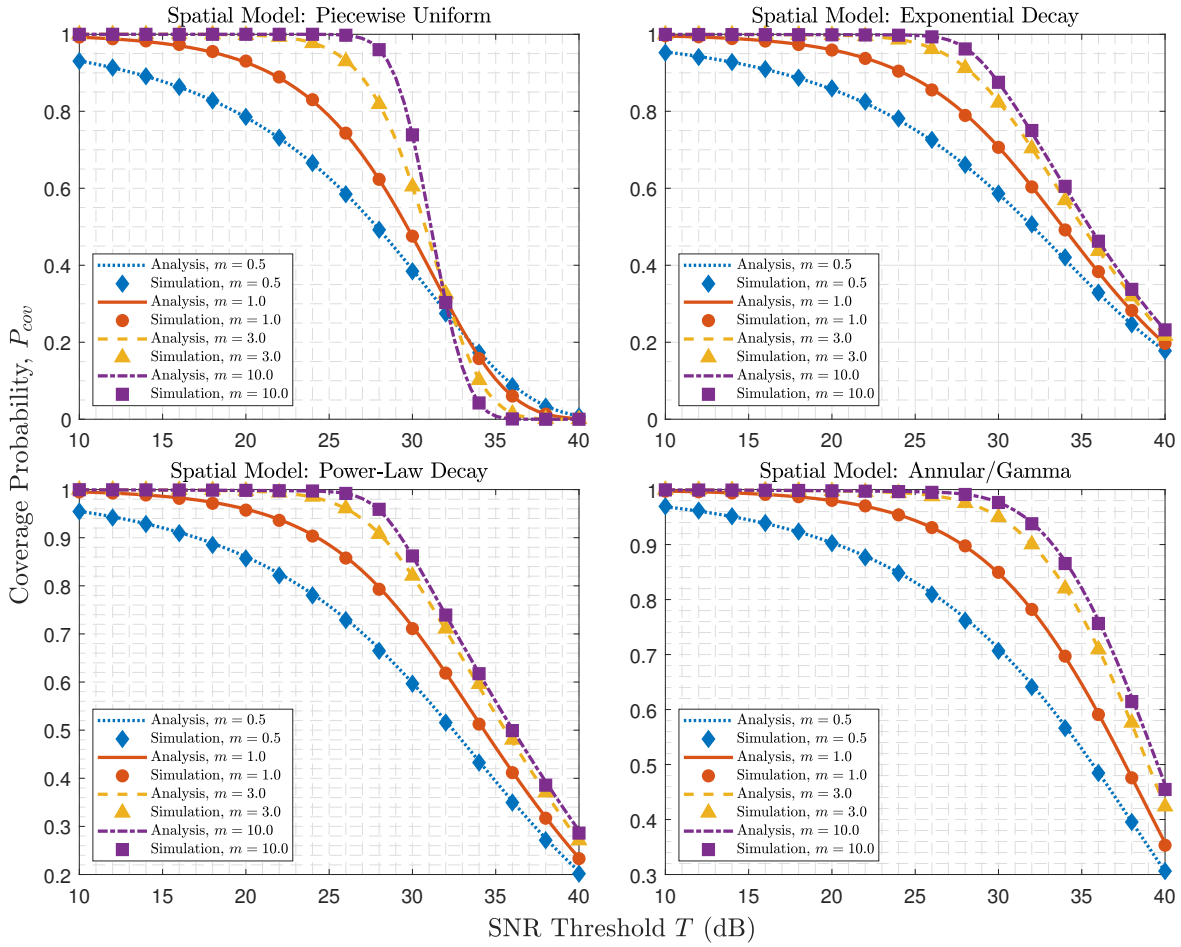

Fig. 2. Average downlink coverage probability as the function of SNR threshold, T, for the four considered spatial distribution models.

diminished performance. This confirms that the physical channel conditions play a significant role in network reliability, a factor accurately captured by our model.

B. The Primacy of Macroscopic Geographical Topology

Fig. 3 transitions from intra-model analysis to a direct comparison of the four spatial models, clearly demonstrating that the macroscopic geographical topology is the primary determinant of network performance. The distinct, non-overlapping performance curves reveal that the choice of spatial distribution is not a minor adjustment but a factor of first-order importance for accurate system analysis.

For a given SNR threshold, the Piecewise Uniform model, which confines vessels to a distant harbor area, exhibits the poorest performance, with its coverage probability declining more rapidly than the other models. In contrast, the Exponential Decay, Power-Law Decay, and Annular/Gamma models, which model more complex and realistic vessel distributions, show markedly superior performance. The inset in Fig. 3 magnifies the performance differences in the critical 29-34 dB SNR range, highlighting the nuanced but significant variations among these more realistic models. This result powerfully substantiates the central thesis that conventional analyses using oversimplified uniform distribution assumptions can lead to significant inaccuracies in performance evaluation.

C. Spatially-Resolved Diagnostics with Coverage Probability Density

While the average coverage probability provides a single, macroscopic performance metric, the Cpdf characterizes the underlying spatial dynamics of the network. As depicted in Fig. 4, the Cpdf is plotted as a function of distance, thereby disaggregating the average performance metric into a spatially-resolved distribution that shows the contribution to coverage from any given distance.

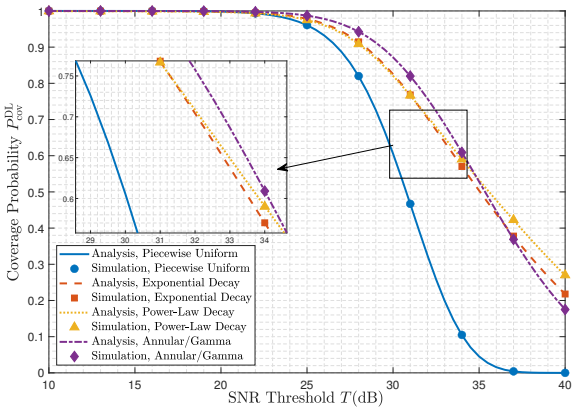

Fig. 3. Average downlink coverage probability as the function of SNR threshold, T, for the four considered spatial distribution models.

Each spatial model exhibits a unique Cpdf signature, which reveals its performance sweet spot—the critical distance where the combination of user density and reliable signal quality is optimal. For instance, the Cpdf for the Exponential Decay model peaks close to the shore, indicating that coverage contributions are highest from the dense concentration of near-shore vessels. The Power-Law Decay model also shows a high contribution from near-shore vessels, but its heavier tail signifies a more sustained contribution from vessels at greater distances, characteristic of a shipping lane. In contrast, the Annular/Gamma model's density peaks significantly offshore, capturing a scenario where traffic is concentrated in a designated operational zone, while the Piecewise Uniform model's contribution is strictly confined to its defined region.

Perhaps the most compelling feature of the Cpdf is its ability to visualize the geographic footprint of physical layer phenomena. As shown in the inset of Fig. 4, the Cpdf reveals sharp, deep dips at specific locations that are not numerical artifacts but the precise geographic footprints of deep fading nulls. These nulls occur at predictable locations where the direct and sea-reflected signal paths interfere destructively, creating zones of near-zero coverage and critical performance bottlenecks. Such crucial, localized information is completely obscured by a single average metric like $P_{\text{cov}}^{\text{DL}}$. The Cpdf, however, makes the precise location and impact of these physical phenomena immediately apparent, providing an unparalleled diagnostic tool for network design and optimization.

VI. Conclusion

This paper has presented a unified framework for analyzing maritime communication networks, leading to two fundamental conclusions. First, we have demonstrated that macroscopic user geography is the dominant factor governing network performance. The choice of a realistic spatial distribution model is not a minor refinement but a first-order necessity for accurate analysis. Second, we have introduced the Cpdf as a powerful diagnostic tool that bridges the gap between macro-level outcomes and their micro-level causes, providing a performance map that identifies critical sweet spots and reveals the precise geographic footprint of physical-layer bottlenecks like multipath fading nulls. Together, these findings advocate for a new paradigm in wireless network analysis: one that prioritizes realistic topological modeling and employs spatially-aware metrics to gain the deep insights necessary for robust system design.

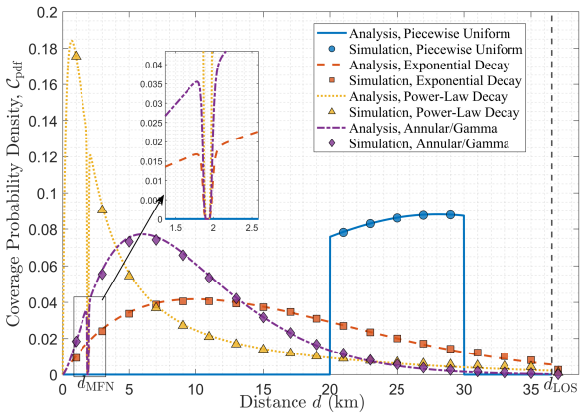

Fig. 4. Downlink coverage probability density as the function of spatial distance d for four distribution model.

References

[1] F. S. Alqurashi, *et al.*, "Maritime communications: A survey on enabling technologies, opportunities, and challenges," *IEEE Internet Things J.*, vol. 10, no. 4, pp. 3525–3547, Feb. 2023.

[2] T. Wei, *et al.*, "Hybrid satellite-terrestrial communication networks for the maritime Internet of Things: Key technologies, opportunities, and challenges," *IEEE Internet Things J.*, vol. 8, no. 11, pp. 8910–8934, Jun. 2021.

[3] J. Wang, *et al.*, "Wireless channel models for maritime communications," *IEEE Access*, vol. 6, pp. 68070–68088, Dec. 2018.

[4] X. Zhang, *et al.*, "Collision-avoidance navigation systems for maritime autonomous surface ships: A state of the art survey," *Ocean Eng.*, vol. 235, Art. no. 109380, pp. 1–22, Sep. 2021.

[5] J. Xu, M. A. Kishk, and M.-S. Alouini, "Space-air-ground-sea integrated networks: Modeling and coverage analysis," *IEEE Trans. Wireless Commun.*, vol. 22, no. 9, pp. 6298–6313, Sep. 2023.

[6] X. Hu, *et al.*, "Performance analysis of end-to-end LEO satellite-aided shore-to-ship communications: A stochastic geometry approach," *IEEE Trans. Wireless Commun.*, vol. 23, no. 9, pp. 11753–11769, Sep. 2024.

[7] W.-Y. Dong, S. Yang, P. Zhang, and S. Chen, "Stochastic geometry based modeling and analysis of uplink cooperative satellite-aerial-terrestrial networks for nomadic communications with weak satellite coverage," *IEEE J. Sel. Areas Commun.*, vol. 42, no. 12, pp. 3428–3444, Dec. 2024.

[8] W.-Y. Dong, S. Yang, P. Zhang and S. Chen, "Modeling and performance analysis of IoT-over-LEO satellite systems under realistic operational constraints: A stochastic geometry approach," *IEEE Internet Things J.*, vol. 12, no. 15, pp. 30576–30593, Aug. 2025.

[9] W.-Y. Dong, S. Yang and S. Chen, "Uplink performance analysis of heterogeneous non-terrestrial networks in harsh environments: A novel stochastic geometry model," *IEEE Trans. on Commun.*, vol. 73, no. 8, pp. 6734–6747, Aug. 2025.

[10] Y. H. Lee, F. Dong, and Y. S. Meng, "Near sea-surface mobile radiowave propagation at 5 GHz: Measurements and modeling," *Radioengineering*, vol. 23, no. 3, pp. 824–830, Sep. 2014.

[11] N. Okati, *et al.*, "Downlink coverage and rate analysis of low earth orbit satellite constellations using stochastic geometry," *IEEE Trans. Commun.*, vol. 68, no. 8, pp. 5120–5134, Aug. 2020.